Plasmonics
DOI 10.1007/s11468-015-0148-3

Illumination Dependent Optical Properties of Plasmonic Nanorods Coupled to Thin-Film Cavities

Xingxing Chen[1] · **Min Qiu**[1,2] · **Richard J. Blaikie**[3] · **Boyang Ding**[3]

Received: 13 September 2015 / Accepted: 26 November 2015

Abstract The scattering spectra and intensity of gold nanorods placed at varied distances above gold films have been simulated and measured under various conditions, demonstrating that scattering characteristics of the nanorod-film system are highly dependent on illumination conditions. Studying the surrounding electric fields of nanorods reveals that the illumination-dependent properties of the system are induced by the interference in the nanorod-film system. Both simulations and experiments show that optimising the nanorod-film distance can greatly enhance scattering magnitudes up to ~20 times for certain illumination conditions. We propose an application of the studied system in facilitating photo-thermal conversion.

Keywords Gold nanorod · Thin-film · Fabry-Perot cavity · Illumination-dependence photo-thermal effect

Electronic supplementary material The online version of this article (doi:10.1007/s11468-015-0148-3) contains supplementary material, which is available to authorized users.

✉ Min Qiu
minqiu@zju.edu.cn

✉ Richard J. Blaikie
richard.blaikie@otago.ac.nz

✉ Boyang Ding
boyang.ding@otago.ac.nz

[1] State Key Laboratory of Modern Optical Instrumentation, Department of Optical Engineering, Zhejiang University, Hangzhou 310027, China

[2] School of Information and Communication Technology, Royal Institute of Technology, Electrum 229, Kista 16440, Sweden

[3] MacDiarmid Institute for Advanced Materials and Nanotechnology, Department of Physics, University of Otago, PO Box 56, Dunedin 9016, New Zealand

Noble metal nanoparticles (NPs) are capable of capturing light and concentrating it to a small volume due to the excitation of localised surface plasmons (LSPs), i.e. collective oscillation of conduction electrons in the NPs. Such plasmonic excitations induce an increase of both scattering and absorption at resonance frequencies and can be influenced by the presence of a nearby metal film. For example, NPs placed at a small distance ($d \leq 30$ nm) away from a metal film using a dielectric spacer can lead to a large field enhancement within the NP-film gap due to the hybridization [1–4] between LSPs on the NPs and surface plasmon polaritons (SPPs) propagating along the adjacent metal films. For larger gap spacing, the interaction between NPs and metal films takes place in complex manners: on one hand, the plasmonic hybridisation reduces as the thickness of the dielectric spacer increases; on the other hand, larger gap spacing leads to interference between NP scattering and reflection from the metal mirror, i.e. LSPs in NPs couple with a Fabry-Perot (FP) like thin-film cavity. As a result of the interplay between these multiple resonances, the NP-cavity system with proper gap spacing can maximise the field enhancement in NPs [5] and narrow down the linewidth of optical resonances [6, 7], thus being widely used to improve the surface-enhanced Raman scattering [8–16] (infrared absorption [17]), optical and chemical sensing [6, 7, 18–27], fluorescence enhancement [28], optical bistability [29] and photoemission [30]. Recently, Wirth et al. have also demonstrated that spectra and directivities of NP scattering can be altered by coupling NPs with interference layers [31].

Previous studies generally focused on the optical properties of NP-cavities at fixed illumination conditions. For example, the field enhancement in arrays of optical antennas placed above a gold mirror has been studied under polarised illumination at normal incidence [5, 6]; or utilising a normal dark-field (DF) microscope, the scattering of single NPs coupled to a thin-film cavity has been

Published online: 08 December 2015

investigated [7, 31] with unpolarized oblique illumination, which is defined by the DF condensor's numerical aperture (NA). However, we want to point out that optical characteristics of metal NPs that are coupled to a cavity can be greatly modified by altering illumination conditions, especially for NPs with anisotropic geometries. This is because (i) it is well-known that the electromagnetic (EM) field distributions in a thin-film cavity are very sensitive to the change of illumination conditions due to interference effects; and (ii) anisotropic NPs, like gold nanorods (AuNRs), show highly polarised resonant behaviours due to the polarised excitation of LSPs in the NPs. As the result, coupling anisotropic NPs with a metal film will further enhance the interplay between the illumination conditions and the excitation of LSPs. Specifically in this report, we demonstrate that the scattering spectra and intensity of single AuNRs above a Au film are significantly influenced by their surrounding EM fields that result from the interference effects in the thin-film cavity; and that varying the gap spacing allows us to flexibly engineer the AuNRs' illumination-dependent scattering behaviours. In addition, both simulated and experimental results show that proper gap spacing and illumination conditions can make the scattering intensity of AuNRs considerably enhanced (larger than ~20 times) compared with AuNRs on their own. Finally, we also discuss the absorption properties of the NR-cavity system and propose its application in photo-thermal conversion.

In our simulations, AuNRs with hemispherical ends were separated from a Au substrate (150 nm thick) with different distances using a dielectric spacer (schematics in Fig. 1). The dielectric constant of Au is taken from Ref. [32] and the geometries of AuNRs were set to be 88 nm in length and 34 nm in width. The refractive index of the dielectric spacer was set to be 1.51 for all wavelengths corresponding to polyvinyl alcohol (PVA) and the spacer thickness is varied from 40 to 210 nm. As shown in the schematics of Fig. 1, the system's optical response was evaluated with three different illumination conditions: polarised plane-wave illumination at normal incidence, oblique illumination with electric field parallel with the substrate (s-polarised, denoted as E_x illumination), and oblique illumination with electric field parallel to the plane of incidence, i.e. the x-z plane (p-polarised, denoted as H_y illumination). The incident angle was set to be $\theta=53^{\circ}$ mimicking the normal DF illumination with NA=0.8. The nanorod is so oriented that the projections of electric fields onto the film surface are parallel to the NR length in each case, thus being capable of efficiently exciting the longitudinal LSPs, which are the primary resonances in AuNRs.

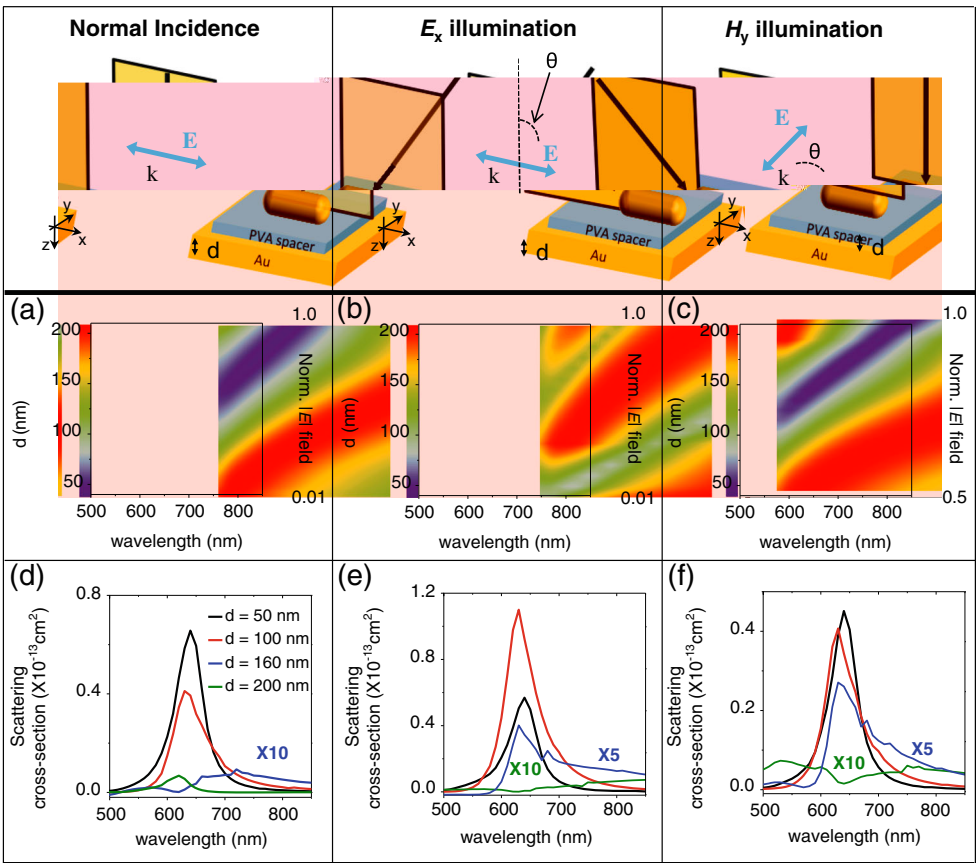

Fig. 1 Magnitudes of electric fields at 17 nm above the spacer layer (centre of AuNRs) in the air as a function of spacer thickness d and wavelength λ under normal incidence (**a**), E_x (**b**) and H_y (**c**) illuminations. Scattering cross-section of AuNRs placed at d=50 (*black line*), 100 (*red line*), 160 (*blue line*) and 200 nm (*green line*) under normal incidence (**d**), E_x (**e**) and H_y (**f**) illuminations. *Top schematics* show configurations for each illumination conditions

According to Ref. [31], the physical process of the interaction between illuminations and AuNR separated from a Au surface by a dielectric spacer can be considered as three successive procedures: (i) light illuminating on the bare thin-film cavity leads to a certain EM field distribution in the cavity as a result of interference between top and bottom reflection; (ii) the resulting EM fields interact with the AuNRs and induce light scattering; (iii) scattered light from the AuNR interferes with the bottom reflection. We have modelled electric fields at the distance of 17 nm from the PVA spacer in the air, which corresponds to the centre position of the studied AuNRs, for different illumination conditions using transfer matrix method [33]. Figure 1a–c demonstrate the magnitudes of electric fields $|E|$, which are normalised to their maximum, as a function of spacer thickness d and wavelength λ for normal incidence, E_x and H_y illumination, respectively. Irrespective of the illumination conditions, $|E|$ vary with both the thickness and wavelength, exhibiting alternations of maxima and minima, which are a clear evidence of interference patterns.

The scattering of AuNRs is evaluated by modelling the scattering cross-section of AuNRs placed at distances (50, 100, 160, and 200 nm) above Au surfaces under normal incidence (Fig. 1d), E_x (Fig. 1e) and H_y illumination (Fig. 1f) using Comsol Multiphysics. For normal incidence, the scattering spectrum of the AuNR at d=50 nm (black line in Fig. 1d) shows a maximum at λ=640 nm with a value of 6.57×10^{-14} cm^2, while the scattering maximum of the AuNR at d=100 nm (red line) slightly blue-shifts to λ=630 nm with a lower magnitude of 4.12×10^{-14} cm^2. Increasing the spacer thickness to d=200 nm (green line) results a further blue-shift of the maximum to λ=620 nm with a much less magnitude (6.79×10^{-15} cm^2). Despite the different magnitudes, the scattering cross-section of AuNRs at d=50, 100 and 200 nm share similar resonant features, i.e. maxima appear at λ~630 nm corresponding to longitudinal LSPs in AuNRs. However, the scattering spectrum for the AuNR at d=160 nm (blue line in Fig. 1d) shows completely different spectral appearance (a minimum at λ=620 nm) and extremely low magnitude (the highest value of 9.34×10^{-16} cm^2 at λ=720 nm). Comparing these spectra with the electric fields $|E|$ (Fig. 1a) reveals that the distance-dependent scattering properties of AuNRs under normal incidence highly relate to the variation of $|E|$ with spacer thicknesses. For example, at λ=630 nm, $|E|$ peaks at d=50 nm, then gradually reduces towards thickness increasing and rises again after d=170 nm, coinciding with the variation of scattering magnitudes of AuNRs above the substrate. We also note that when d=160 nm, the spectrum of $|E|$ shows a minimum at λ~620 nm, which exactly corresponds to the scattering minimum of the AuNR 160 nm above the Au film.

Illuminating the NR-cavity with oblique incidence (θ=53°), e.g. E_x illumination (Fig. 2e), immediately alters the scattering cross-section of AuNRs coupled to a Au substrate. In this case, the scattering of the AuNR at d=50 nm acquires higher magnitude than that of the AuNR at d=100 nm. It is also worth noting that under E_x illumination, the AuNR at d=160 nm has a scattering maximum at λ=630 nm, whereas scattering of the AuNR at d=200 nm shows a minimum at the same wavelength, which is completely opposite to the case under normal incidence (Fig. 1d). Comparing with $|E|$ (Fig. 1b) reveals that the modifications of scattering spectra are highly relevant to the electric fields distribution above the thin-film cavity too. For example, the scattering minimum of the AuNR at d=200 nm corresponds to the minimum in the $|E|$ spectrum at d=200 nm. The scattering spectra of cavity-coupled AuNRs under H_y illumination (Fig. 1f) share similar resonant characteristics with those under E_x illumination.

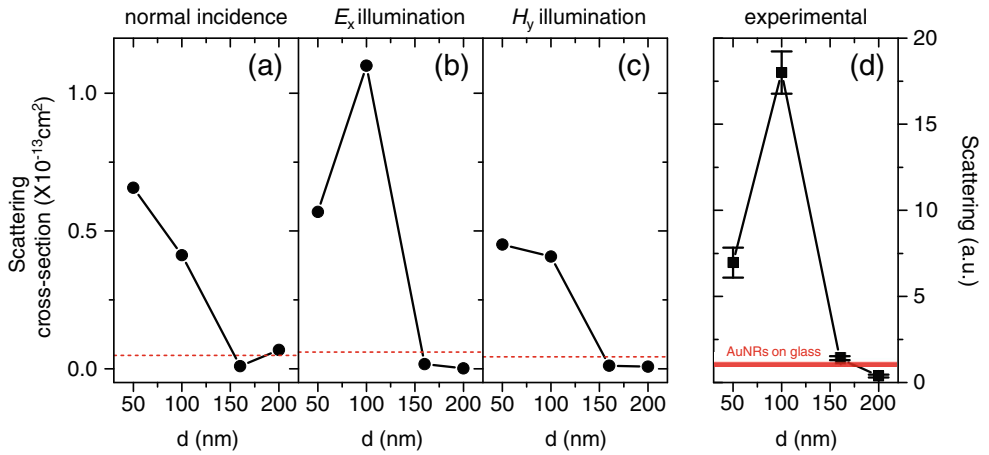

Fig. 2 Magnitudes of scattering maxima for AuNRs at varied distances above a Au substrate under normal incidence (**a**), E_x (**b**) and H_y (**c**) illuminations. *Dashed line* in each panel indicates the scattering magnitude of AuNRs on a glass substrate under the same illumination conditions. **d** Experimentally acquired scattering magnitudes of AuNRs placed at different distances above a Au substrate under DF illumination with NA=0.8. *Thick red line* indicates the scattering magnitude of AuNRs on a glass substrate. The width of the red line refers to statistical variation of the magnitudes

However, it is also noted that the scattering of AuNR at d=160 nm (blue line in Fig. 1f) shows a second maximum at λ=530 nm with a low magnitude (4.67×10^{-16} cm^2). This is induced by the vertical excitation of LSPs as reported elsewhere [31] and can only be excited under H_y (p-polarised) illumination. The scattering cross-sections of cavity-coupled AuNRs perpendicular to the projections of electric field onto the film surface have also been simulated, but not shown here (please see Fig. S1 in Appendix materials) due to their extremely low scattering intensity (two orders of magnitudes lower than the displayed results).

In general, Fig. 1 reveals that the scattering characteristics of the cavity-coupled AuNRs highly relate to the electric fields that result from the interference effects in the thin-film cavity, thus making the scattering spectra and intensity of the NR-cavity very sensitive to the change of illumination conditions. On the other hand, the interaction between the Au film and AuNRs allows us to modify such illumination-dependent scattering properties by adjusting the NR-film distance. Figure 2a–c demonstrate the magnitude variation of scattering maxima for AuNRs at different distances above a Au film under normal incidence, E_x and H_y illumination, respectively. The magnitudes of these scattering maxima were obtained from the scattering cross-section shown in Fig. 1. As shown in the spectra of Fig. 1, the scattering magnitudes of AuNRs vary with the NR-film distance and the illumination conditions. Specifically, as compared to the AuNRs on glass substrate (red dashed line in each panel of Fig. 2), the scattering maxima for AuNRs at d=50 and 100 nm have been significantly enhanced irrespective of the illumination conditions, which correspond to the positions where the field enhancement in AuNRs can be optimised [5]. Especially for the AuNR at d=100 nm above a Au substrate under E_x illumination (Fig. 2b), the scattering is ~20 times higher than that of the AuNR on a glass film.

We also want to mention that the variation of scattering magnitudes with NR-film distance has been observed in our experiment too. Figure 2d shows the measured scattering magnitudes for single AuNRs at d=50, 100, 160 and 200 nm above a Au substrate using dark-field microscopy. (For details of the sample preparation, experimental set-up, scattering spectra, far-field and scanning microscope images of AuNRs, please see Fig. S2 and S3 in Appendix materials). In our experiment, unpolarised white light shines on the sample from all azimuthal directions but in a narrow range of the incident angle (θ=53°), similar to the ensemble effect of E_x and H_y illumination. In order to verify the reproducibility, we have measured the scattering spectra of over 30 single AuNRs for each spacer thickness. The geometry differences between AuNRs and rough spacer surfaces lead to slight fluctuations of scattering magnitudes for AuNRs at the same NR-film distance. However, the tendency of magnitudes variation with spacer thickness greatly resembles the simulated result under E_x illumination (Fig. 2b), exhibiting the dominant strength of longitudinal LSPs in AuNRs. It is also noted that the scattering enhancement as compared to the AuNRs on glass substrate is even larger than the simulated results, suggesting a great potential of this cavity-coupled field enhancement technique in practical applications.

It is also well known that the LSPs contribute to the increase of light absorption in metallic NPs, which leads to an application in photo-thermal conversion, since the absorbed light can be converted into thermal energy giving rise to a temperature increase of NPs. The metal-insulator-metal (MIM) absorbers have been widely used to improve the heating or annealing process of metallic NPs. However, the traditional configuration of MIM absorbers generally acquires ultrathin gap spacing ($d\leq$10 nm) between NPs and metal films to excite strong plasmonic resonances within the gap [34, 35], thus facilitating the dissipation of absorbed light into thermal energy. To illustrate this, we have modelled the absorption cross-sections of the AuNR placed at d=10 nm above a Au film (blue line in Fig. 3) and the AuNR on a glass substrate (green line in Fig. 3) under various conditions, with normal incidence illumination shown in Fig. 3a. We note that

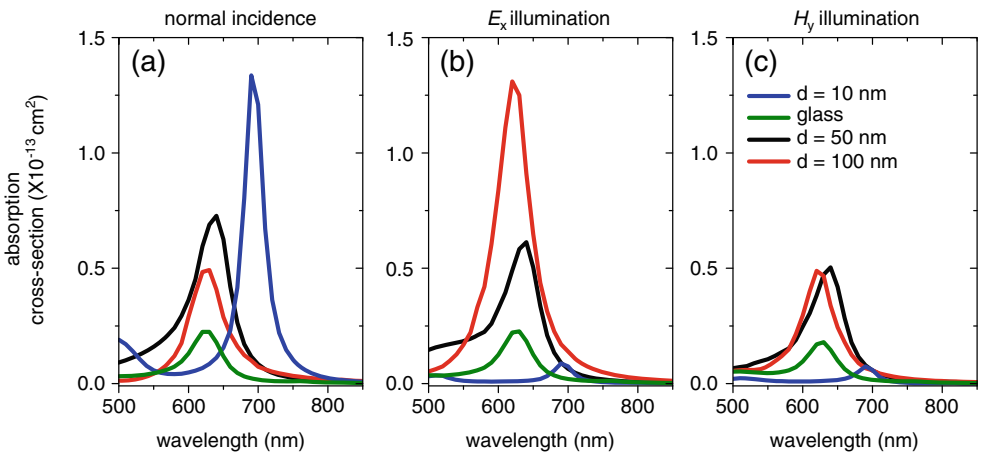

Fig. 3 Absorption cross-section of AuNRs placed at d=50 nm (*black line*), 100 nm (*red line*), 10 nm (*blue line*) and glass (*green line*) under normal incidence (**a**), E_x (**b**) and H_y (**c**) illuminations

the strong field enhancement within the NR-film gap results in a ~6 times higher and red-shifted absorption maximum at λ=690 nm as compared to that of the AuNR on glass, demonstrating the excellent capability of ultrathin gap spacing MIM configuration to enhance light absorption. However, the absorbing behaviours of the traditional MIM designs are significantly dependent on the illumination conditions. For example, under E_x (Fig. 3b) and H_y (Fig. 3c) illuminations, the absorption magnitudes of the AuNR at d=10 nm (blue line) rapidly reduce down to ~1/15 of the absorption under normal illumination, even lower than the absorption of AuNRs on glass substrate. Such absorbing characteristics will undoubtedly compromise the practical application of traditional MIM design in photo-thermal conversion, because most of the heating experiments [34–38] have been carried out using a focused laser beam through a microscope objective, such as the DF illumination used in our experiments, which leads to significant oblique components in the focused beam. In this context, we propose that the NP-cavity configuration may provide another option for NP heating, especially for illuminations focused by high NA objectives for following reasons:

(i) Coupling NPs to a thin-film cavity can also increase the NP absorption by optimising the field enhancement in the NPs. For example, as shown in Fig. 3a, the absorption cross-sections of AuNRs placed at d=50 (black line) and 100 nm (red line) demonstrate that the cavity-coupled AuNRs gain lower but the same order of absorption magnitudes as does the AuNR at d=10 nm under normal illumination.
(ii) Under oblique illumination conditions (Fig. 3b, c), the cavity-coupled AuNRs acquire much higher absorption.
(iii) Adjusting the spacer thickness allows us to flexibly engineer the absorption characteristics of the system, e.g. for the AuNR at d=50 nm, the absorption maximum remains at ~0.6×10^{-13} cm^2 immune to illumination directions; while for the AuNR at d=100 nm, the absorption maximum can be enhanced up to 1.31×10^{-13} cm^2 for E_x illumination.
(iv) According to our previous study [39], for traditional MIM absorber based on gap resonances, smaller gap spacing results in better absorption magnitudes, which will complicate the fabrication of the dielectric spacer. This drawback can be avoided for the NP-cavity configuration as it has much more tolerance to spacer thickness.

In order to verify our proposal, we have simulated the relative energy transfer ΔE in AuNRs placed at d=10, 50 and 100 nm from a Au film and a glass substrate under normal incidence, E_x and H_y illumination, as shown in Table 1. The simulations were preformed using COMSOL Multiphysics with the Heat Transfer Model: Heat Transfer in Solids (Stationary) [34]. Specifically, $\Delta E=E_{tot}-E_{exch}$ refers to the energy transfer in a AuNR to achieve thermal equilibrium with surroundings under optical illumination, while the NR-cavity system was initially placed at room temperature (T=300 K); where E_{tot} is the total energy the AuNR absorbs from the illumination and E_{exch} refers to the heat exchange between the AuNR and surroundings (air, the PVA spacer and Au film) during the heating process. The illumination wavelength was chosen to match the spectral position of the maximum of absorption cross-section of each sample. Specifically, λ=690 nm for the AuNR at d=10 nm, λ=630 nm for d=50 nm, and λ=620 nm for d=100 nm and the glass substrate sample. The incident power of all illumination was fixed at 0.03 mW/um^2 that is a relatively low value for photo-thermal conversion.

Table 1 Relative energy transfer ΔE in AuNRs placed at different distances above a Au film and a glass substrate under different illumination conditions but with the same illumination power 0.03 mW/μm^2. The AuNRs were initially placed at room temperature environment (T=300 K)

Sample	Illumination		
	Normal	E_x	H_y
d=10 nm	16.57 fJ	1.17 fJ	0.99 fJ
d=50 nm	13.33 fJ	11.36 fJ	9.25 fJ
d=100 nm	9.99 fJ	24.07 fJ	9.48 fJ
Glass	3.73 fJ	3.71 fJ	2.96 fJ

For the traditional MIM absorber (d=10 nm), the relative energy transfer in the AuNR is ΔE=16.57 fJ. for normal incidence and is significantly reduced to ΔE=1.17 fJ. and ΔE=0.99 fJ. for E_x and H_y illumination in accordance with the reduced absorption. In the case of d=50 nm, the relative energy transfers are ΔE=13.33 fJ, ΔE=11.36 fJ. and ΔE=9.25 fJ. for corresponding illumination conditions, complying with the almost identical absorption magnitudes for these three illuminations. For d=100 nm, the relative energy transfer is increased up to ΔE=24.07 fJ. for E_x illumination, exhibiting that the absorption of the NR-cavity system can be flexibly tuned by adjusting the spacer thickness.

In conclusion, we present a numerical study of the illumination-dependent scattering properties of AuNRs that are coupled to a thin-film cavity. Specifically, we have modelled the scattering spectra of AuNRs placed at varied distances from a Au substrate under different illumination conditions, demonstrating that both the scattering spectra and magnitudes significantly vary with the polarisation and angle of the illuminations. Comparing with the surrounding electric fields of AuNRs reveals that the scattering characteristics of the NR-cavity system are highly influenced by the interference effects in the thin-film cavity, thus making the system sensitive to illumination conditions. In addition, both

simulations and experiments show that optimising the NR-film distance can greatly enhance the scattering intensity up to ~20 times for certain illumination conditions. In the end, we propose an application of the studied structure in photothermal conversion, illustrating that the NR-cavity system acquires much better capability to facilitate the heating or annealing of metallic NPs than the traditional MIM absorbers. In addition to the discussed application in heating process, our study can also contribute to the design of optical antennas [5]. For example, coupling optical antennas to a proper thin-film cavity can improve the antennas' capturing efficiency to signals from certain or even all directions.

Figure S1 demonstrates the simulated scattering cross-section of AuNRs placed at different distances above a Au substrate under normal incidence (a), E_y (b) and H_x (c) illumination. In these situations, the projections of the electric field onto the film surface are perpendicular to the NR length. The overall scattering intensities are two orders of magnitudes lower than those under illumination with the parallel projections of electric fields onto the film surface parallel to the NR length, which are discussed in the main text.

Dark-field microscopy has usually been used to measure the scattering properties of single NPs. In a normal reflection dark-field microscope, unpolarised light was focused on a single NP by a dark-field condenser, thus making the illumination becomes an up-polarised and oblique plane-wave from all azimuthal directions (Fig. S2). To obtain the scattering properties of a NP measured by dark-field microscopy, we calculate the total scattering cross-section of AuNRs above a Au substrate by superimposing their scattering cross-section from all azimuthal illuminations, i.e. E_x, E_y, H_x and H_y as shown in Fig. 1 and Fig. S1. The simulated total scattering cross-sections of AuNRs placed at different distances above a Au surface are demonstrated in Fig. S3a. The scattering of the AuNR d=50 nm (black line) from the Au film has a maximum at λ=640 nm with a value of 1.0×10^{-13} cm^2, while the maximum of scattering of d=100 nm slightly blue-shifts to λ=630 nm but with higher scattering magnitude (1.51×10^{-13} cm^2). In contrast, the scattering from AuNRs d=160 (blue line) and 200 (green line) nm above a Au film acquires much lower magnitudes. Normalising the scattering spectra to their maxima make the resonant features better observable (Fig. S3b). In addition to the highest maximum at λ=630 nm, the scattering of the AuNR 160 nm above a Au film has second peak at λ= 520 nm. It is also noted that the scattering of the AuNR 200 nm above a Au surface peaks at λ=530 nm and shows a rising trend towards the long wavelength region.

In order to confirm the simulations, we have also measured the scattering spectra of AuNRs placed at different distances above a Au surface (Fig. S3b–h). The AuNRs with an average geometry ~85 nm in length and ~35 nm in width were prepared using a seed mediated method [40]. The surfaces of AuNRs have been modified with Poly(sodium 4-styrenesulfonate) (PSS, Mw ~700,000), so they can be dispersed in ethanol without aggregation. The Au substrates were prepared by coating 120 nm thick Au films on smooth silicon wafers using electron beam evaporation. PVA films with different thickness were then spin-coated on the Au substrates as spacers. The thickness of PVA spacers can be controlled by either adjusting the concentration of PVA in aqueous solution or changing the spinning speed and are confirmed by a surface profilometer (Dektak-XT). AuNRs dispersed in ethanol suspension are drop-casted on different substrates. A reflection dark-field microscope (Nikon, ECLIPSE 80) was used to measure the scattering spectra of individual AuNRs. White-light illumination from a halogen lamp is focused on the samples by a dark-field condenser, and the scattered light was collected by an objective (Nikon, CFI LU Plan Epi ELWD, 100X, NA=0.8). The scattering spectra were recorded using a fibre-based spectrometer (Ocean Optics, QE65 pro), while scattering image was taken by a CCD camera (Nikon, DIGITAL CAMERA HEAD DS-Fi1). Left panels in Fig. S3e–h show the scattering images of AuNRs placed at d=50, 100, 160, and 200 nm above a Au surface, respectively, while the right panels show the scanning electron microscopy (SEM) images of the red circle marked scattering patterns, the scattering spectra of which in each image are demonstrated in Fig. S3c. The experimentally acquired scattering spectra share great similarities to the simulated results shown in Fig. S3a in intensity variation. The detailed resonant features that can be clearly seen from the normalised spectra (Fig. S3d) are also similar to the simulated results. The general red-shifts of the experimental spectra with respect to the simulated ones are the result of variations in the geometry of AuNRs and spacer thickness. It is noted that doughnut-shape green patterns centred with red colour can be observed from the scattering image of AuNRs d=160 nm above a Au surface (Fig. S3g), indicating the excitation of vertical oriented dipole moments for green light. This corresponds to the maximum at λ= 530 nm in the scattering spectra (blue line in Fig. S3a–d).

Acknowledgments This work was financially supported by New Zealand's Marsden Fund through contract UOO-1214, the Priming Partnership Pilot Funding (University of Otago), the National Natural Science Foundation of China (grants 61275030, 61205030, and 61235007), the Open Fund of State Key Laboratory of Advanced Optical Communication Systems and Networks, and the Swedish Foundation for Strategic Research (SSF) and the Swedish Research Council (VR).

References

1. Nordlander P, Prodan E (2004) Plasmon hybridization in nanoparticles near metallic surfaces. Nano Lett 4:2209–2213

2. Mock JJ, Hill RT, Degiron A, Zauscher S, Chilkoti A, Smith DR (2008) Distance-dependent plasmon resonant coupling between a gold nanoparticle and gold film. Nano Lett 8:2245–2252
3. Hu M, Ghoshal A, Marquez M, Kik PG (2010) Single particle spectroscopy study of metal-film-induced tuning of silver nanoparticle plasmon resonances. J Phys Chem C 114:7509–7514
4. Chen X, Yang Y, Chen Y-H, Qiu M, Blaikie RJ, Ding B (2015) Probing plasmonic gap resonances between gold nanorods and a metallic surface. J Phys Chem C 119:18627–18634
5. Seok TJ, Jamshidi A, Kim M, Dhuey S, Lakhani A, Choo H, Schuck PJ, Cabrini S, Schwartzberg AM, Bokor J, Yablonovitch E, Wu MC (2011) Radiation engineering of optical antennas for maximum field enhancement. Nano Lett 11:2606–2610
6. Ameling R, Langguth L, Hentschel M, Mesch M, Braun PV, Giessen H (2010) Cavity-enhanced localized plasmon resonance sensing. Appl Phys Lett 97:253116
7. Schmidt MA, Lei DY, Wondraczek L, Nazabal V, Maier SA (2012) Hybrid nanoparticle–microcavity-based plasmonic nanosensors with improved detection resolution and extended remote-sensing ability. Nat Commun 3:1108
8. Shoute LCT (2010) Multilayer substrate-mediated tuning resonance of plasmon and SERS EF of nanostructured silver. ChemPhysChem 11:2539–2545
9. Min Q, Pang Y, Collins DJ, Kuklev NA, Gottselig K, Steuerman DW, Gordon R (2011) Substrate-based platform for boosting the surface-enhanced Raman of plasmonic nanoparticles. Opt Express 19:1648–1655
10. Ahmed A, Gordon R (2011) Directivity enhanced Raman spectroscopy using nanoantennas. Nano Lett 11:1800–1803
11. Ahmed A, Gordon R (2012) Single molecule directivity enhanced Raman scattering using nanoantennas. Nano Lett 12:2625–2630
12. Wang D, Zhu W, Chu Y, Crozier KB (2012) High directivity optical antenna substrates for surface enhanced Raman scattering. Adv Mater 24:4376–4380
13. Wang D, Zhu W, Best MD, Camden JP, Crozier KB (2013) Directional Raman scattering from single molecules in the feed gaps of optical antennas_si_001.pdf. Nano Lett 13:2194–2198
14. Wang D, Zhu W, Best MD, Camden JP, Crozier KB (2013) Wafer-scale metasurface for total power absorption, local field enhancement and single molecule Raman spectroscopy. Sci Rep 3:2867
15. Ahmed A, Pang Y, Hajisalem G, Gordon R (2012) Antenna design for directivity-enhanced Raman spectroscopy. Int J Opt. doi:10.1155/2012/729138
16. Milekhin AG, Yeryukov NA, Sveshnikova LL, Duda TA, Rodyakina EE, Gridchin VA, Sheremet ES, Zahn DRT (2015) Combination of surface- and interference-enhanced Raman scattering by CuS nanocrystals on nanopatterned Au structures. Beilstein J Nanotechnol 6:749–754
17. Brown LV, Yang X, Zhao K, Zheng BY, Nordlander P, Halas NJ (2015) Fan-shaped gold nanoantennas above reflective substrates for surface-enhanced infrared absorption (SEIRA). Nano Lett 15:1272–1280
18. Schalkhammer T, Lobmaier C, Pittner F, Leitner A, Brunner H, Aussenegg FR (1995) The use of metal-island-coated pH-sensitive swelling polymers for biosensor applications. Sens Actuators B Chem 24:166–172
19. Schalkhammer T, Lobmaier C, Pittner F, Leitner A, Brunner H, Aussenegg FR (1995) Metal island coated polymer sensor for direct determination of the volume effect of chaotropic agents. Mikrochim Acta 121:259–268
20. Bauer G, Pittner F, Schalkhammer T (1999) Metal nano-cluster biosensors. Mikrochim Acta 131:107–114
21. Mayer C, Stich N, Palkovits R, Bauer G, Pittner F, Schalkhammer T (2001) High-throughput assays on the chip based on metal nano-cluster resonance transducers. J Pharm Biomed 24:773–783
22. Palkovits R, Mayer C, Bauer G, Winkler H, Pittner F, Schalkhammer T (2003) Structural behavior of nanometric carbohydrate films transduced by a resonant technique. Biopolymers 69:333–342
23. Hiep HM, Yoshikawa H, Saito M, Tamiya E (2009) An interference localized surface plasmon resonance biosensor based on the photonic structure of Au nanoparticles and SiO2/Si multilayers. ACS Nano 3:446–452
24. Kuchler I, Pittner F, Pittner G, Sontag G (2010) Development of a metal-island-coated swelling/shrinking copolymer sensor for measurement of divalent metal ions. Monatsh Chem 141:131–135
25. Sannomiya T, Balmer TE, Hafner C, Heuberger M, Vörös J (2010) Optical sensing and determination of complex reflection coefficients of plasmonic structures using transmission interferometric plasmonic sensor. Rev Sci Instrum 81:053102
26. Li G, Chen X, Li O, Shao C, Jiang Y, Huang L, Ni B, Hu W, Lu W (2012) A novel plasmonic resonance sensor based on an infrared perfect absorber. J Phys D Appl Phys 45:205102
27. Lee M, Jeon H, Kim S (2015) A Highly Tunable and Fully Biocompatible Silk Nanoplasmonic Optical Sensor. Nano Lett 15:3358–3363
28. Fernandez-Garcia R, Rahmani M, Hong M, Maier SA, Sonnefraud Y (2013) Use of a gold reflecting-layer in optical antenna substrates for increase of photoluminescence enhancement. Opt Express 21:12552–12561
29. Butet J, Martin OJF (2014) Manipulating the optical bistability in a nonlinear plasmonic nanoantenna array with a reflecting surface. Plasmonics 10:203–209
30. Fang Y, Jiao Y, Xiong K, Ogier R, Yang Z-J, Gao S, Dahlin AB, Käll M (2015) Plasmon Enhanced Internal Photoemission in Antenna-Spa